Al fraction induced effects on the capacitance characteristics of n⁺-GaN/$Al_xGa_{1-x}N$ IR detectors

Laura E. Byrum[a], Gamini Ariyawansa[a], Ranga Jayasinghe[a], Nikolaus Dietz[a], A. G. Unil Perera[a], Steven G. Matsik[b], Ian T. Ferguson[c], Andrew Bezinger[d], and Hui Chun Liu[d]

[a]Department of Physics and Astronomy, Georgia State University, Atlanta, Georgia 30303, USA;
[b]NDP Optronics LLC, Mableton, Georgia 30126, USA;
[c]School of Electrical and Computer Engineering, Georgia Institute of Technology, Atlanta, Georgia 30332, USA:
[d]Institute for Microstructural Sciences, National Research Council, Ottawa K1A OR6, Canada

ABSTRACT

Capacitance-voltage-frequency measurements on n^+-GaN/$Al_xGa_{1-x}N$ Heterojunction Interfacial Workfunction Internal Photoemission (HEIWIP) detectors were used to analyze the effects of Al fraction induced heterojunction barrier and its effect on the electrical characteristics at the heterointerface. The detector's IR threshold can be modified by changing the barrier Al concentration. A sample with an Al fraction of 0.1 shows a distinct capacitance step and capacitance hysteresis, which is attributed to N-vacancies and/or C-donor electron trap states located just above the Fermi level (200 meV) at the GaN/AlGaN interface, with activation energies of 149±1 and ∼189 meV, respectively. A sample with an Al fraction of 0.026 showed negative capacitance and dispersion, indicating interface electron trap states located below the Fermi level (88 meV), most likely due to C-donor and/or N-vacancy with activation energies of 125±1 and 140±2 meV, respectively. Additional impurity related absorption centers were identified in both samples, however these shallow Si-donor sites (∼30.9±0.2 meV) did not affect the capacitance as these states were located in the barrier layer and not in the vicinity of the Fermi level. The Al fraction in the barrier layer was found to significantly change the positions of the interface trap states relative to the Fermi level, resulting in the observed capacitance characteristics.

Keywords: UV-IR dual band detector, GaN/AlGaN, Heterojunction, Interface traps, Negative capacitance, Capacitance hysteresis

1. INTRODUCTION

The wide band gap of GaN enables the fabrication of unique IR detectors, suited for applications such as space situational awareness, flame detection, military sensing, and industrial applications. Such IR detectors are radiation-hard, solar blind, and relatively resistant to thermal carrier emission and interband tunneling.[1,2] High-quality GaN based device structures are presently limited by the presence of trap states at interface junctions, induced either by lattice mismatch, interface roughness, or interfacial bonding mismatch.[3]

Here, the effects of Al concentration in the barrier layer of n^+-GaN/$Al_xGa_{1-x}N$ dual-band UV-IR detectors as analyzed by capacitance-voltage (C-V) and -frequency (C-f) measurements are discussed. The GaN-based dual-band detector was developed[4] to operate simultaneously or separately in both the infrared (IR) and ultraviolet (UV) ranges. The IR detection is based on the intraband transition from the n^+-GaN emitter,[2] while UV detection is based on interband transitions in the AlGaN barrier.[4]

2. DUAL-BAND UV-IR DETECTOR: STRUCTURE AND DETECTION MECHANISM

The detector structures were grown by low pressure Metal-Organic Chemical Vapor Deposition (MOCVD) on a *c*-plane sapphire substrate. As shown in Fig. 1(a), the device structures consist of a 0.2 μm n^+-GaN top contact (emitter) layer, a 0.6 μm $Al_xGa_{1-x}N$ barrier layer, and a 0.7 μm n^+-GaN bottom contact layer. The $Al_xGa_{1-x}N$

Nanophotonics and Macrophotonics for Space Environments III, edited by Edward W. Taylor, David A. Cardimona, Proc. of SPIE Vol. 7467, 74670W · © 2009 SPIE · CCC code: 0277-786X/09/$18 · doi: 10.1117/12.828156

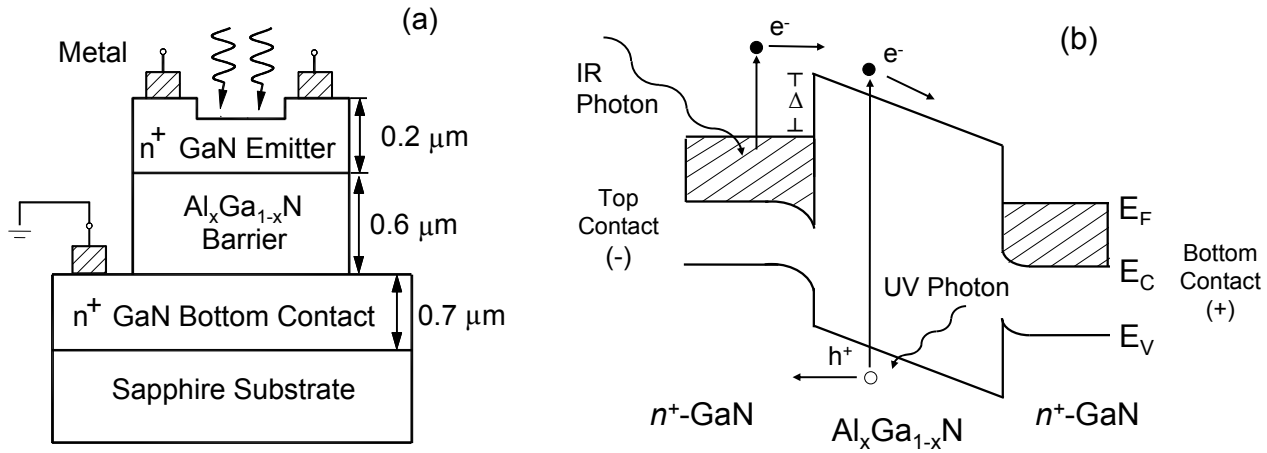

Figure 1. (a) The structure of the dual-band detector consists of an undoped $Al_xGa_{1-x}N$ barrier layer located between n^+-GaN top and bottom contact layers. Sample 1547 and sample 1158 have Al fractions of 0.1 and 0.026, respectively. Both n^+-GaN layers are doped with Si to a concentration of 5×10^{18} cm^{-3}. When the sample is negatively biased, the top contact layer will act as an emitter. (b) The dual-band detector operates by collecting carriers from intraband IR transitions and interband UV transitions. The work function Δ is 88 meV for sample 1158 and 200 meV for sample 1547.

barrier layers in sample 1547 and sample 1158 have Al fractions of 0.1 and 0.026, respectively. The top and bottom contact layers in both sample series are n^+-doped with silicon to a doping concentration of 5×10^{18} cm^{-3}.

Using dry etching techniques, square mesas were formed by removing the area between the metal ring contacts. The GaN layer under the metal contacts remained unetched (0.2 μm thick). Thus, even in the fully-etched sample GaN is still present between the metal contacts and the AlGaN barrier, as the GaN layer has to remain between the metal contact and the AlGaN barrier for carriers to be collected.

The detector responds to IR radiation through a three stage process: free carrier absorption, internal photoemission, and (under an external electric field) collection of emitted carriers at the contact. A schematic of the detection mechanism is depicted in Fig. 1(b).

The use of different band-gap materials for the emitter and barrier layers in the detector introduces a workfunction Δ (in meV)defined as the offset between the Fermi level in the n^+-GaN emitter layer and the conduction band in the $Al_xGa_{1-x}N$ barrier. This workfunction determines the IR threshold wavelength λ_0 (in μm), as an IR response is only possible if the photoexcited carries are able to surmount the barrier.

$$\lambda_0 = 1240/\Delta \tag{1}$$

In a heterostructure, the workfunction is determined by the band gap offsets from both doping Δ_d and Al fraction Δ_x:

$$\Delta = \Delta_d + \Delta_x. \tag{2}$$

Due to the high doping concentration in the contact layers, the Fermi level lies above the conduction band minimum. Thus, the n^+-GaN/$Al_xGa_{1-x}N$ interface is analogous to a metal-semiconductor interface, as the doping concentration exceeds the Mott transition in n^+-GaN.

UV light detection takes place in the AlGaN barrier layer when an absorbed photon generates an electron-hole pair through the interband transition of the photoexcited electron from the valence band to the conduction band. Assisted by an external electric field, the carriers will be transported out of the UV-active barrier region and collected at the contacts. The UV threshold wavelength λ_{0G} (in nm) is dependent on the barrier layer bandgap, given by

$$\lambda_{0G} = 1240/E_G \tag{3}$$

where E_G is the bandgap between the valence and conduction bands[5] in $Al_xGa_{1-x}N$ is

$$E_G = 6.13x + 3.42(1-x) - 1.08x(1-x). \quad (4)$$

Variations in the barrier layer Al content, as well as the contact layer doping concentration will change the UV and IR threshold. At present, however, the increased Al content has been found[3] to contribute to a significant number of interfacial defect states that limits the detector performance.

3. CAPACITANCE PROFILES

C-V and C-f measurements were carried out using a computer controlled Hewlett-Packard 4284A LCR meter. Capacitance scans were run from -2 V to +2 V at frequencies between 100 Hz and 1 MHz. When forward biased, the top contact is positive and the bottom contact is negative. Under reverse bias the top contact is negative and the bottom contact is positive.

Frequency-dependent capacitance dispersion (FDCD) was observed in C-V profiles for sample 1547 and sample 1158, as shown in Fig. 2(a) and 2(c), and has been attributed to the presence of frequency-dependent trap states at the interface. FDCD has been observed in other GaN/AlGaN heterojunctions such as Schottky diodes[3] and heterojunction field effect transistors (HFETs)[6] between 10 kHz and 1 MHz.

In addition to FDCD, negative capacitance was observed in the C-V profiles of sample 1158 for frequency values of 10 kHz, 100 kHz, and 500 kHz, which is consistent with the frequency range of ∼6 - 600 kHz where

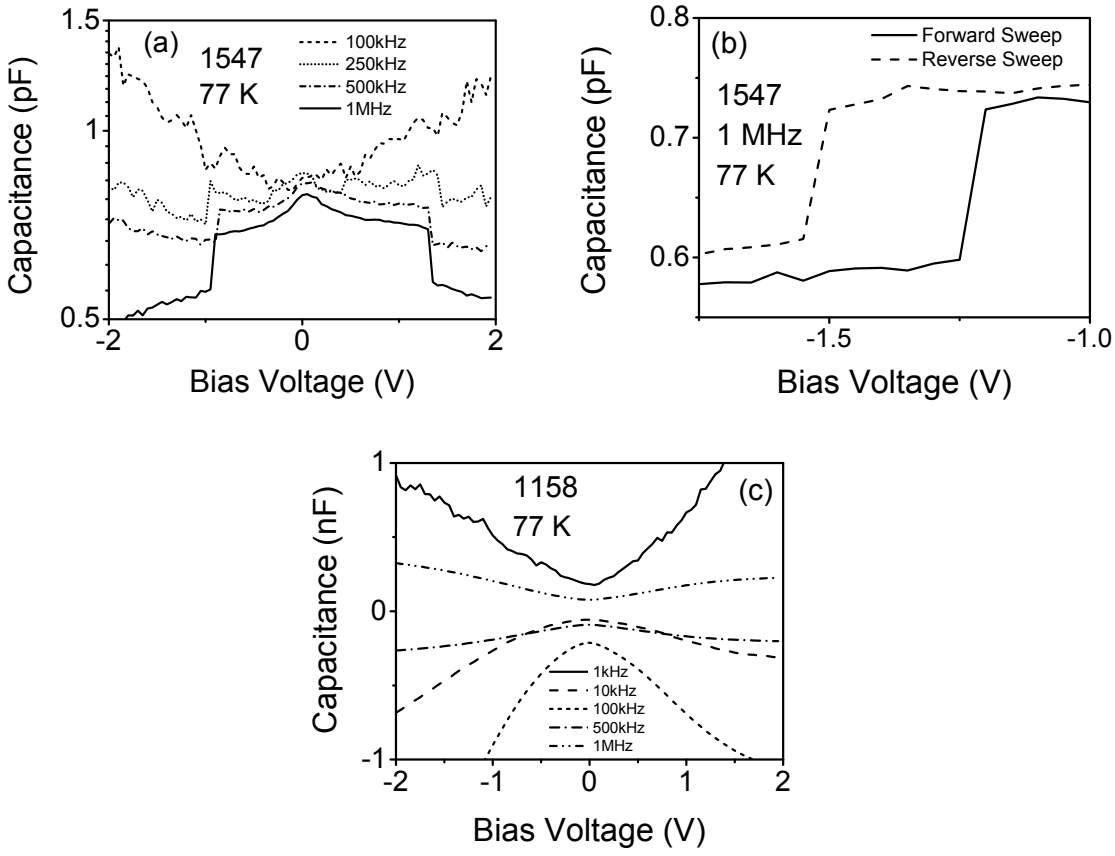

Figure 2. Capacitance-voltage profiles for sample 1547 showing (a) frequency-dependent capacitance dispersion and a capacitance-step. The capacitance-step became more pronounced as frequency increased. (b) The capacitance hysteresis between forward and reverse scans. The vertical offset between forward and reverse scans is within the noise range. (c) Sample 1158 exhibited FDCD and negative capacitance.

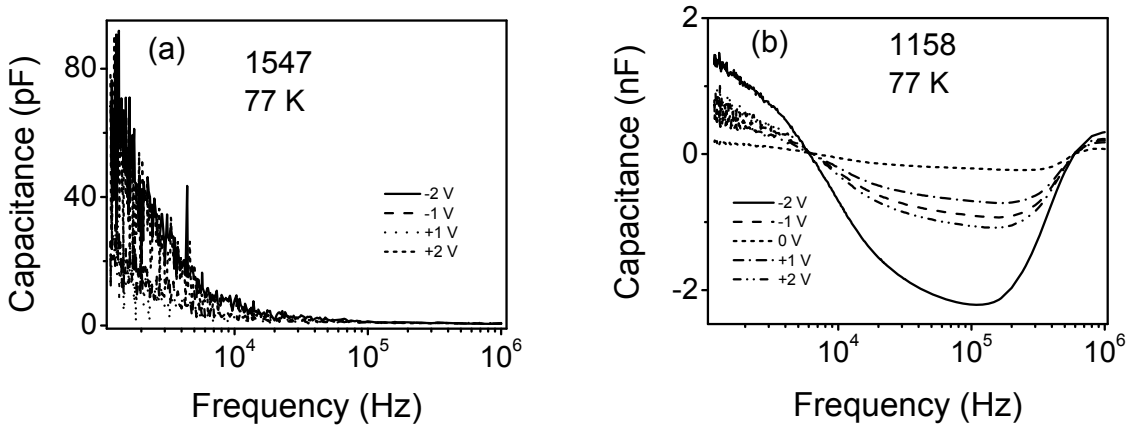

Figure 3. Due to finite inertia, (a) sample 1547 exhibited an exponential decrease in capacitance with increasing frequency. (b) FDCD and negative capacitance were observed in the C-f profile of sample 1158. From the C-f profile, $1/f$ inverse relaxation times of $\sim 1.77 \pm 0.05$ μs and 155 ± 9 were calculated from the points where the capacitance transitioned from negative to positive or positive to negative.

negative capacitance occurred in the C-f scans. Negative capacitance has been observed in various other detector structures.[7,8,9] The phenomenon has been attributed to carrier generation and recombination due to interfacial defect states, most likely due to the presence of occupied trap states at the emitter intrinsic layer interface.[7] Due to the symmetry in the C-V profiles for both forward and reverse biasing, it is assumed that the processes responsible for negative capacitance and FDCD are present at both heterointerfaces.

In the C-f profiles of sample 1547, shown in Fig. 3(a), the measured capacitance for all bias values approached the geometrical capacitance of the structure as the frequency was increased. This is a result of the carrier transport process reaching a maximum value due to finite inertia when the frequency exceeds the inverse relaxation time.[7] Additionally, at high frequencies and low bias, the voltage changes too rapidly for impurities to react. As the frequency decreases, the defect induced trap states have time to become charged and the capacitance begins to increase.

3.1 Capacitance Hysteresis

The capacitance-steps and capacitance hysteresis observed in the C-V profile of sample 1547, shown in Fig. 2(a) and 2(b), are due to an abrupt change in carrier occupation at the n^+-GaN/AlGaN interface. The presence of C-donor/N-vacancy induced defect bands located slightly above the Fermi level are assumed to provide the necessary electron recombination sites.

Under zero bias the defect states lie above the Fermi level and are unoccupied. Applying a bias across the structure will cause the Fermi level to shift relative to its equilibrium position, and at a critical value of ther Fermi level, the defect induced trap states will be filled. The abrupt capacitance-step occurs when carriers are able to occupy the (previously unoccupied) trap states. Similarly, when the Fermi level decreases below the trap state levels, the capacitance will abruptly decrease, as these states are no longer occupied. The band diagrams corresponding to the structure of sample 1547 (including the position of trap states) under zero bias and reverse bias are shown in Fig. 4(a) and 4(b), respectively.

The presence of the capacitance hysteresis requires an additional factor. With the abrupt change in carrier concentration, as the Fermi level moves into the defect states with increasing bias, an accumulation region will form due to the build-up of negative charges at the interface. This accumulation region lowers the effective field at the interface, and as the scan direction is reversed, a higher voltage will be required to empty the initially filled trap states. Thus the capacitance-step occurs at a higher bias. Due to the initial carrier occupation, the capacitance-step will occur at different values for forward and reverse scans, resulting in the observed capacitance hysteresis.[13]

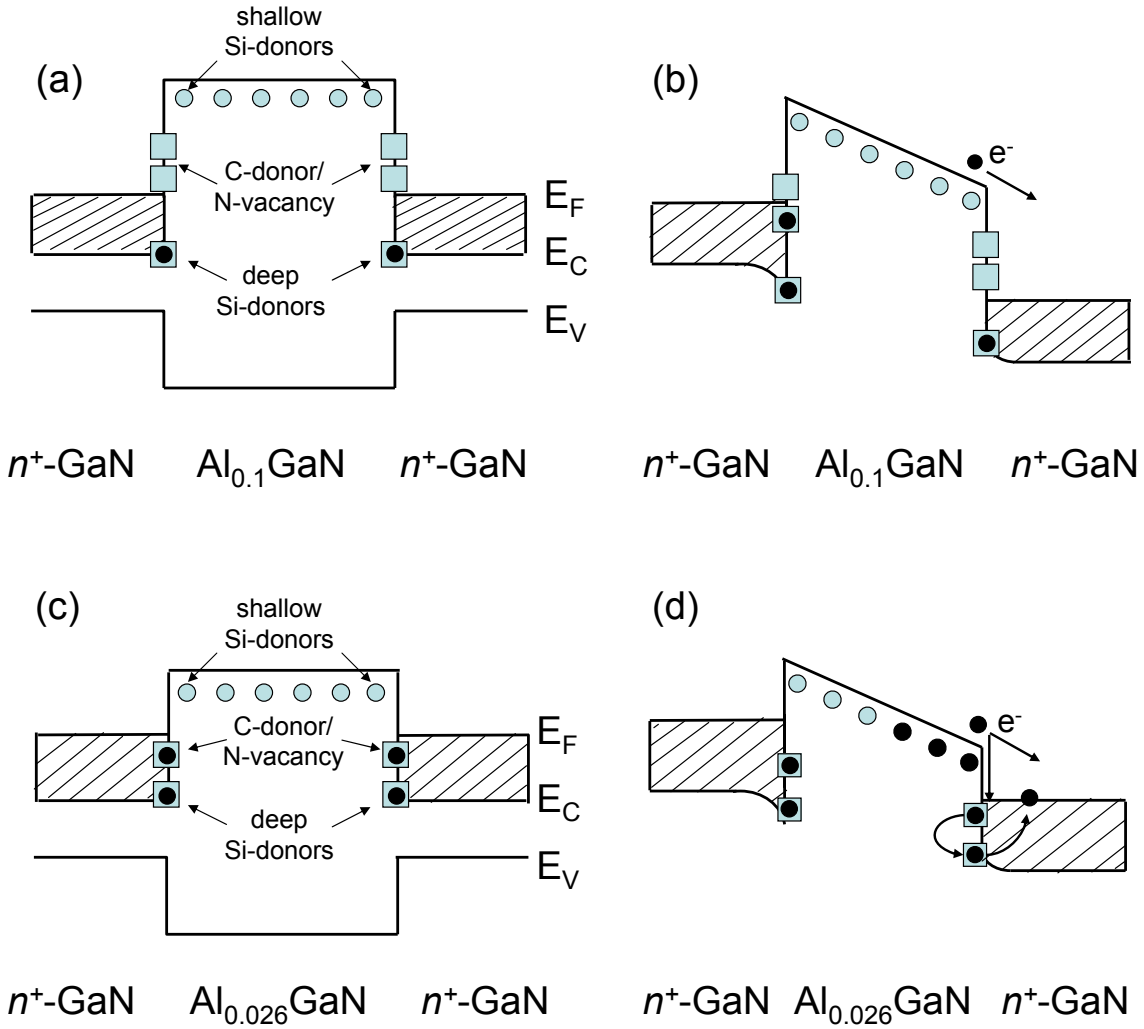

Figure 4. Band diagram of sample 1547 at (a) zero bias and (b) negative bias. At zero bias the C-donor/N-vacancy defect trap states are located above the Fermi level. As the bias became more negative, the Fermi level moved through the interface defect states, causing the abrupt increase/decrease in capacitance. Band diagram of sample 1158 with (c) zero bias and (d) negative bias. When sample 1158 is negatively biased the C-donor/N-vacancy and deep Si-donor defect trap states are located below the Fermi level. In the figure, the GaN top contact is to the left of the intrinsic AlGaN barrier layer and the GaN bottom contact is to the right; the diagram is intended to show the area between the metal contacts.

3.2 Negative Capacitance

Negative capacitance was observed in the C-f profile of sample 1158, shown in Fig. 3(b). The $1/f$ relaxation times of 155 ± 9 and 1.77 ± 0.05 μs were extrapolated from the frequencies where the capacitance transitioned from positive to negative (∼6 kHz) and negative to positive (∼600 kHz), respectively. The slower relaxation time is attributed to shallow Si-donor trap states above the Fermi level, pinned to the AlGaN barrier. C-donor/N-vacancy and deep Si-donor traps (pinned at the emitter layer) located below the Fermi level were related to the faster relaxation times.

At sufficiently low frequency, both generation and recombination processes are occurring simultaneously. Once the frequency reaches ∼6 kHz, the shallow Si-donor related defect states above the Fermi level, with slower relaxation times, become saturated and will no longer contribute to the capacitance. The C-donor/N-vacancy and deep Si-donor related trap states with faster relaxation times will provide the dominant contribution to the net capacitance. Because these states act as electron recombination centers, a negative capacitance is observed. Once the frequency reaches ∼600 kHz, these faster trap states will also become saturated and the capacitance will return to a positive value. As the frequency is increased further, the capacitance will approach the geometrical capacitance of the system, as both the generation and recombination processes are inactive.

The band diagrams, including the location of the defect trap states under both zero bias and reverse bias are depicted in Fig. 4(c) and (d), respectively. Under an applied bias, electrons with sufficient energy will traverse the AlGaN barrier or fill available trap energy states above the Fermi level at the heterointerface. However, in the presence of the C-donor/N-vacancy and deep Si-donor trap states below the Fermi level, electrons with sufficient energy are able to dislocate electrons already present in the trap states. This process is analogous to impact ionization or the Auger effect. Once these trap states become ionized, they provide a site for electron recombination. If the interface charge density variation is reversed, the capacitance can become negative.[14]

4. EFFECTS OF BARRIER ALUMINUM CONCENTRATION

In the IR spectra of sample 1547 and sample 1158, shown in Fig. 5, the free carrier response peaks are observed between 3-8 μm and 8-14 μm, respectively, consistent with the Al fractions of 0.1 and 0.026. In sample 1547, a broad impurity related response peak is also present in the 8-13 μm range. The impurity related absorption centers with transitional energy of 112 ± 0.5 and ∼142 meV, correspond to activation energies of 149 ± 1 and ∼189 meV, respectively. C-donor/N-vacancy impurities at the heterointerface with defect states above the Fermi level are thought to account for the states with activation energies of 149 ± 1 meV. The origin of the defect states associated with an activation energy of 149 ± 1 meV is still unknown, but could possibly be due to deep Si-donor impurities at the heterojunction.

In sample 1158, defect related absorption peaks are observed superimposed on the free carrier response between 11 and 13.6 μm. Based on previous reports,[10,11,12] the defect related absorption peak with a transitional energy of approximately 93.4 ± 0.5 meV, corresponding to an activation energy of 125 ± 1 meV, is attributed to C-donor/N-vacancy impurities at the heterointerface. The peak with a transitional energy of 105 ± 1.5 meV and activation energy of 140 ± 2 meV is attributed to deep Si-donor states at the heterointerface, pinned to the defect energy band in the emitter layer. The conduction band offset at the n^+-GaN/AlGaN heterointerface for the 1158 sample was 137 ± 7 meV, which is consistent with the activation energy of 140 ± 2 meV.

For both samples, an absorption peak corresponding to a defect energy state with a 1s-2p± transitional energy of 23.2 ± 0.1 meV (sample 1547) and 23.1 ± 0.1 meV (sample 1158) was observed at ∼54 μm and was attributed to shallow Si-donor impurities in the AlGaN barrier layer. The presence of these trap states with almost identical activation energies indicates that while the barrier Al fraction changes the barrier height and location of interface trap states, it does not effect the location of the shallow Si-donor impurities in the barrier. A summary of sample parameters and associated defect state energies in provided in Table 1.

Both samples investigated show similar defect energy states, regardless of Al fraction. However, the response of the C-donor/N-vacancy and deep Si-donor related states to an applied bias, as observed in the C-V and C-f profiles, was different. Even though changes in Al fraction did not introduce new trap states, the conduction band offset was altered, resulting in changes in the position of the Fermi level relative to the trap states.

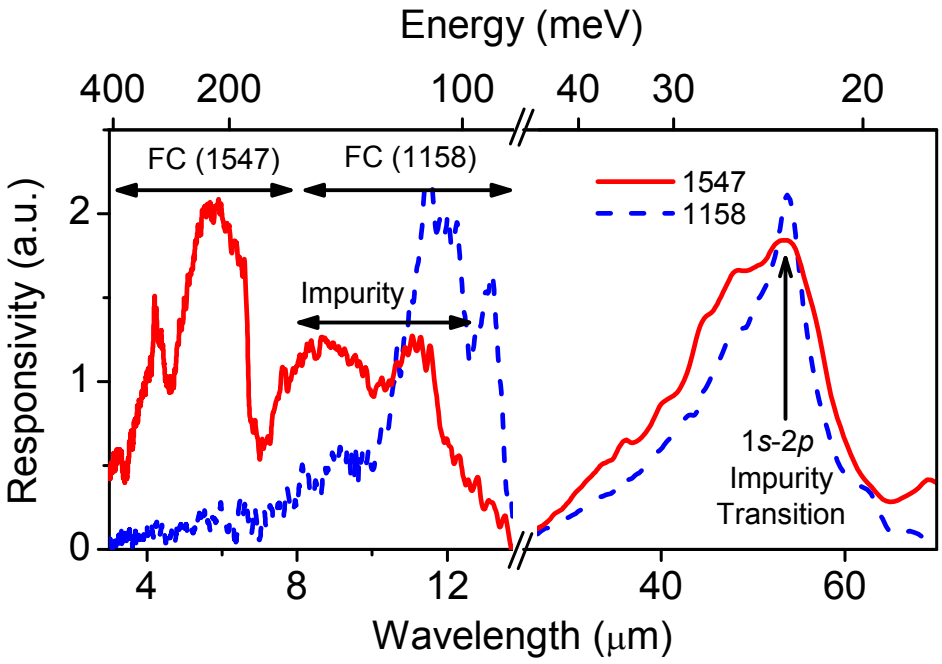

Figure 5. IR spectra showing the free carrier (FC) response peaks between 3-8 μm and 8-14 μm for sample 1547 and sample 1158, respectively. Defect related absorption centers with transitional energies of 112 $\pm$ 0.5 and $\sim$142$\pm$ meV (corresponding to activation energies of 149 $\pm$ 1 and $\sim$189 meV, respectively) were observed in sample 1547 and attributed to C-donor/N-vacancy and deep Si-donor states. In sample 1158, C-donor/N-vacancy and deep Si-donor states had transitional energies of 93.4 $\pm$ 0.5 and 105 $\pm$ 1.5 meV, corresponding to activation energies of 125 $\pm$ 1 and 140 $\pm$ 2 meV, respectively. Shallow Si-donor states in the AlGaN barrier with $1s$-$2p_{\pm}$ transitional energy of 23.2 $\pm$ 0.1 meV (sample 1547) and 23.1 $\pm$ 0.1 meV (sample 1158) were observed in both samples.

The Al concentration of sample 1547 (0.1) resulted in a workfunction of 200 meV, positioning the Fermi level below the C-donor/N-vacancy trap states. Under an applied bias, the Fermi level can be moved through the defect energy states causing abrupt changes in the carrier concentration, resulting in the observed capacitance-step and capacitance hysteresis. Due to the conduction band offset in sample 1547, calculated to be 248 $\pm$ 6 meV, the deep Si-donor related states are pinned to the GaN layer and are therefore not active in the process responsible for the capacitance-step or capacitance hysteresis. Additionally, because of the large energy difference between the deep Si-donor states (below E_F) and the C-donor/N-vacancy, negative capacitance does not occur, even when the C-donor/N-vacancy states are below the Fermi level.

Due to the low Al fraction in sample 1158 (0.026), the workfunction was reduced to 88 meV, resulting in the Fermi level lying above the C-donor/N-vacancy and deep Si-donor trap states. Since the Fermi level consistently remained above the trap states, these defect energy states were always occupied, and no abrupt change in carrier concentration occurred. Thus, no capacitance-step or capacitance hysteresis was observed. However, negative capacitance was observed in both the C-V and C-f profiles of sample 1158 due to an impact ionization-like process between the trap states at the heterointerface, below the Fermi level.

5. CONCLUSIONS

IR spectroscopy revealed three impurity related absorption centers that were related to shallow Si-donor (pinned to the AlGaN barrier layer), C-donor/N-vacancy, and deep Si-donor impurities (pinned at the GaN contact layer). The activation energies of the C-donor/N-vacancy trap states in sample 1547 indicate that they are located at the heterointerface, just above the Fermi level (200 meV), whereas, the C-donor/N-vacancy related defect states in sample 1158 are located at the heterointerface, just below the Fermi level (88 meV).

Table 1. Summary of sample parameters and defect related activation energies. In sample 1547, all defect states were located above the Fermi level, whereas in sample 1158, all defect states were located below the Fermi level.

	Sample Number	
	1547	1158
Al fraction	0.10±0.001	0.026±0.001
Work function (meV)	200±2	88±2
Conduction band offset (meV)	248±6	137±7
Free carrier response (μm)	3-8	8-13
Shallow Si-donor (meV)	30.9±0.1	30.8±0.2
C-donor/N-vacancy (meV)	149±1	125±1
Deep Si-donor (meV)		140±2
Unknown (meV)	∼189	

For low Al fractions (0.026), negative capacitance results from C-donor/N-vacancy and deep Si-donor traps at the heterointerface with activation energies below the Fermi level. At higher Al fractions (0.1), C-donor/N-vacancy defect energy states are present at the heterointerface just above the Fermi level, resulting in the observed capacitance step and capacitance hysteresis due to charge accumulation. Shallow Si-donor impurities in the AlGaN barrier layer with activation energies above the Fermi level were present in both samples, regardless of Al fraction.

The Al fraction in the barrier layer contributes to the conduction band offset at the n^+-GaN/$Al_xGa_{1-x}N$ heterojunction. As the Al fraction is varied, a significant change in the positions of these interface trap states relative to the Fermi level was found, resulting in the observed capacitance characteristics.

ACKNOWLEDGMENTS

Work supported in part by the US Air Force under Small Business Innovation Research Program (SBIR) contract # FA9453-06-C-005, US National Science Foundation, and GSU MBDAF.

REFERENCES

[1] E. Munoz, E. Monroy, J. L. Pau, F. Calle, F. Omnes, and P. Gibart, "III nitrides and UV detection," J. Phys.: Condens. Matter, **13**, 7115 (2001).

[2] G. Ariyawansa et al., "GaN/AlGaN heterojunction infrared detector responding in 8-14 and 20-70 μm ranges," Appl. Phys. Lett., **89**, 141122 (2006).

[3] R. M. Chu, Y. G. Zhou, K. J. Chen, and K. M. Lau, "Admittance characterization and analysis of trap states in AlGaN/GaN heterostructures," phys. stat. sol. (c), **0**, 2400 (2003).

[4] G. Ariyawansa et al., "GaN/AlGaN ultraviolet/infrared dual-band detector," Appl. Phys. Lett., **89**, 091113 (2006).

[5] U. Ozgur, G. Webb-Wood, H. O. Everitt, F. Yun, and H. Morkoc, "Systematic measurement of $Al_xGa_{1-x}N$ refractive indices," Appl. Phys. Lett., **79**, 4103 (2001).

[6] W. L. Liu, Y. L. Chen, A. A. Balandin, and K. L. Wang, "Capacitance-Voltage Spectroscopy of Trapping States in GaN/AlGaN Heterostsructure Field-Effect Transistors," J. Nanoelectron. Optoelectron., **1**, 258 (2006).

[7] A. G. U. Perera, W. Z. Shen, M. Ershov, H. C. Liu, M. Buchanan, and W. J. Schaff, "Negative Capacitance of GaAs Homojunction Far-Infrared Detectors," Appl. Phys. Lett., **74**, 3167 (1999).

[8] M. Ershov, H. C. Liu, L. Li, M. Buchanan, Z. R. Wasilewski, and V. Ryzhii, "Unusual capacitance behavior of quantum well infrared photodetectors," Appl. Phys. Lett., **70**, 1828 (1997).

[9] X. Wu, E. S. Yang, and H. L. Evans, "Negative capacitance at metal-semiconductor interfaces," J. Appl. Phys., **68**, 2845 (1990).

[10] W. J. Moore, J. A. Freitas, and R. J. Molnar, "Zeeman spectroscopy of shallow donors in GaN," Phys. Rev. B, **56**, 12073 (1997).

[11] M. Sumiya, K. Yoshimura, K. Ohtsuka, and S. Fuke, "Dependence of impurity incorporation on the polar direction of GaN film growth," Appl. Phys. Lett., **76**, 2098 (2000).

[12] V. Bougrov, M. Levinshtein, S. Rumyantsev, and A. Zubrilov, *Properties of Advanced Semicondutor Materials*, (New York: Wiley, 2001).

[13] L. E. Byrum et al., "Capacitance hysteresis in GaN/AlGaN heterostructures," J. Appl. Phys., **105**, 023709 (2009).

[14] L. E. Byrum et al., "Negative capacitance in GaN/AlGaN heterostructure dual-band detectors," J. Appl. Phys. (submitted).